

Influence of composition on the *in-vitro* bioactivity of bioglass prepared by a quick alkali-mediated sol–gel method

M.I. El-Gohary¹, Khairy M. Tohamy¹, M.M. El-Okr², Ashraf F. Ali³, Islam E. Soliman^{1*}

1. Biophysics branch, Faculty of Science, Al-Azhar University, Nasr City 11884, Cairo, Egypt.
2. Physics Department, Faculty of Science, Al-Azhar University, Nasr City 11884, Cairo, Egypt.
3. Inorganic Chemistry Department, National Research Center, Tahreer St., Dokki, Cairo, Egypt.

islamsoloiman@yahoo.com

Abstract: Bioactive glass with composition SiO₂, Na₂O, CaO, P₂O₅ with MgO additive were synthesized through a quick alkali mediated sol–gel method. MgO was substituted for SiO₂ in glass formula up to 5 wt% and *in-vitro* bioactivity of the samples (precipitation behavior of carbonated apatite likely bone layer) was evaluated by soaking them in simulated body fluid (SBF). The characterizations were carried out using XRD, FT-IR, TGA, and DSC. The thermal results showed that all organic and inorganic precursors were completely decomposed before 600 °C and, hence, all glass samples were stabilized at this temperature. The results obtained showed that MgO doping to glass samples increased its degradation and the formation of apatite like bone is delayed.

[El-Gohary MI, Tohamy KM, El-Okr MM, Ali AF, Soliman IE. **Influence of composition on the *in-vitro* bioactivity of bioglass prepared by a quick alkali-mediated sol–gel method.** *Nat Sci* 2013;11(3):26-33]. (ISSN: 1545-0740). <http://www.sciencepub.net/nature>. 4

Key words: bioactive glass, sol-gel, *in-vitro*, bioactivity

1. Introduction

Ca–Si-based bioactive glasses have been studied in last decades, since Hench, (1970) first investigated bioglass. Due to their good bioactivity, such as osteoconductivity and biodegradability ^[1, 2], bioactive glass was used as a bioactive material for bone repair or regeneration ^[3]. In addition bioactive glass is the most of bioactive materials, which could bond to hard and soft tissue ^[4]. When this bioactive glass was soaked into physiological solutions, silica gel layer with high surface area will be firstly formed on the material's surface by partial glass network dissolution and surface polycondensation. It has been recognized that the silica gel layer plays an important role in the nucleation and crystal growth of hydroxycarbonate apatite (HCA) layer ^[5].

Sol–gel technique, as a chemical method, exhibits more interest and provides an available way to synthesize bioactive glass. When compared with the traditional melting method, sol–gel technique has the advantage of lower reaction temperature and allows one to obtain glass which owns higher purity, large surface area, better homogeneity and microporosity ^[6]. However, the particle size of the traditional sol–gel-derived bioactive glasses was bigger than 1 μm ^[7]. In addition, the time of the synthesis of bioactive glasses by traditional sol–gel process is quite long process, because of the delayed gelation and ageing time. Magnesium is

one of the main trace metallic elements existing in human body and it has been shown that it plays an important role in human bone development, maintenance and repair through osteoblastic cell stimulation ^[8]. The aim of the present work is to prepare Mg containing-bioactive-glass by a quick alkali-mediated sol–gel method. The size of the bioactive glass particles will be controlled by using ethanol as dispersant agent to adjusting the pH value of the sol ^[9]. The objectives of this research work are to synthesize and characterize the different compositions (x=0, 1, 3 and 5 wt%) of MgO substituted bioactive glass powders (55-xSiO₂–35CaO–xMgO–5Na₂O–5P₂O₅) with the presence of other modifier for better understanding changes occurred in physicochemical properties of bioglass.

2. Materials and Methods

Tetraethyl orthosilicate (TEOS), calcium nitrate tetrahydrate Ca(NO₃)₂·4H₂O, sodium nitrate NaNO₃, magnesium nitrate hexahydrate Mg(NO₃)₂·6H₂O and triethyl phosphate (TEP) ≥ 98% were purchased from Buchs, Switzerland. Ammonia solution, 33%, and nitric acid, 68%, were purchased from Merck, USA. Both nitric acid and ammonia solutions were diluted to 2M using distilled water.

2.1. Sol-gel synthesis of magnesium-doped bioactive glass

Bioactive glass containing 0, 1, 3 and 5 wt% of MgO were synthesized through a quick alkali-mediated sol-gel technique [7,10]. MgO was added to the glass compositions at the expense of SiO₂. Table (1) presented the nominal compositions and codes of the prepared bioactive glass. Initially, tetraethyl orthosilicate, distilled water and 2M nitric acid (as a hydrolysis catalyst), were successively mixed in ethanol and the mixture was allowed to react for 60 min under continuous magnetic stirring for the acid hydrolysis of TEOS. Then appropriate amounts of series reagents were added in the following sequence: (TEP), Ca(NO₃)₂·H₂O, NaNO₃ and Mg(NO₃)₂·6H₂O, allowing 30 min for each reagent to react completely. After the final addition, mixing of all reagents continued for 60 min to complete hydrolysis. Ammonia solution of 2M concentration (a gelation catalyst) was dropped into the mixture. The mixture was then agitated with glass rod (like as mechanical stirrer) to prevent the formation of a bulk gel. Finally, each prepared gel was dried at 75 °C for 2 days in a drying oven. According to the results of the thermal analysis of the dry gels, which showed that there was no further weight loss above 600 °C, the gels were stabilized by heat treatment, at a constant heating rate of 10 °C min⁻¹ up to 600 °C.

Table 1. The nominal compositions and codes of the prepared magnesium doped sol-gel bioactive glasses

Samples code notification	Composition				
	SiO ₂	Na ₂ O	CaO	P ₂ O ₅	MgO
SPM ₀	55	5	35	5	0
SPM ₁	54	5	35	5	1
SPM ₃	52	5	35	5	3
SPM ₅	50	5	35	5	5

S (silica), P (phosphorus), M (magnesium)

2.2. Characterization

Thermogravimetric analyses (TGA), and differential calorimetric analyses (DSC) were performed for the dried gels using a computerized SETARAM labsys™ TG-DSC thermal analysis system. Scans were performed in the atmosphere, and in a temperature range of 50–1000 °C, at a rate of 10 °C min⁻¹. The materials were analyzed using aluminum oxide powder as a reference. The phase analysis of the samples was examined by X-ray diffractometer, model BRUKERaxs,

using Ni-filtered CuKα irradiation at 40 kV and 25 mA. The infrared spectra of the prepared glass were obtained using Fourier transform infrared spectrophotometer (FT-IR) (Model 580, Perkin-Elmer). Each sample used for infrared spectroscopic analysis was prepared according to KBr technique.

2.3. In-vitro assays in SBF

In vitro assays were performed in a simulated body fluid (SBF), proposed by Kokubo et al. [11]. The SBF solution has a composition and concentration similar to those inorganic parts of human plasma. During soaking process, each disc was soaked into 50 ml SBF contained in a polyethylene bottle. These bottles were covered with a tight lid and placed in thermodynamic incubator (shaking-water bath) at 37 °C for different time periods (control, 7, 15 and 30 days). After being soaked, the powders were rinsed with deionized water and acetone and dried at room temperature.

3. Results and Discussion

3.1. Thermal analysis

Thermogravimetric analysis (TGA) and differential scanning calorimetric (DSC), analysis curves for sample (SPM₃) are shown in Fig. (1a, b). The TGA curves of all samples showed three main stages of weight losses as the heating process proceeded from room temperature up to 1000 °C. Those weight losses appeared at the temperature intervals of 30–130, 130–320, and 320–620 °C for all samples. The first stage was attributed to the removal of water which appears as (humidity and physically adsorbed water) from the surface and any the residual alcohol in the pores of the dried gel [12]. This stage was reflected in the DCS curves of sample (SPM₃) as the first large endothermic peak centered at about 130 °C [13], as shown in Fig. (1a).

The second stage was reflected in the exothermic peaks centered at around 270 °C on the DSC curve of sample (SPM₃), which is most likely due to desorption of chemically adsorbed water [14]. This peak comes from the esterification reaction during condensation of Si-OH groups in the sol-gel network structure [15]. The third stage shown by the TGA curve of sample (SPM₃) which can be accounted by the decomposition of nitrates (NO₃⁻) and ammonia (NH₄). This may be related to endothermic peak located at 495 °C on the DSC curve of sample (SPM₃) [16].

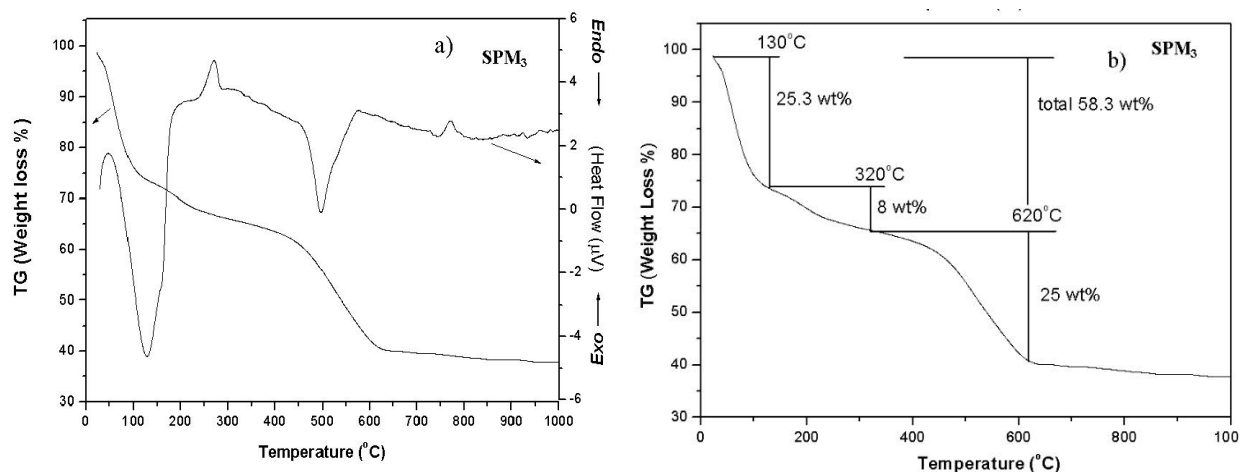


Figure 1. TGA and DSC curves of the sample (SPM₃) gel powder after 120^o C for two days.

A final, and well-defined, exothermic peak appeared on the DSC curves which appears in all samples is located at 825, 783, 770 and 768^oC, for samples SPM₀, SPM₁, SPM₃ and SPM₅, respectively. This was due to transformation of the glass into glass-ceramic. This can be explained as follows; when MgO is substituting SiO₂ it can act as the nucleating agents and decrease the barrier energy of crystallization. This then leads to relieve the rigidity of the glass structure and causes the disruption in the network structure by newly forming ionic bonds between Mg and oxygen (Si–O–Mg) in SiO₄ tetrahedrons in the glassy network [17]. These ionic bonds are weaker than the bonds formed between the two silicon ions and oxygen (Si–O–Si) in the glassy network structure (silicate chain) and therefore, a reduction in T_c was observed. This reduction shift leads to phase transition temperatures to a lower value [18], as shown in Fig. (2).

3.2. X-ray diffraction Analysis

Fig. (3) Shows the XRD pattern obtained for the investigated sample surfaces before the in vitro dissolution test. This figure shows that all the unsoaked prepared glass is completely amorphous in nature, characterized by absence of diffraction peaks only amorphous hump in each glass analyzed which confirms the internal disorder and the absence of any crystalline phase [19].

However, after the immersion in the SBF, the typical diffraction pattern of crystalline hydroxyapatite appeared with strong peaks at 2θ of 22.9^o, 26^o, 31^o and 32^o developed after soaking in SBF for period of 30 days. These observed four peaks of Fig. (4) are assigned

to (1 1 1), (0 0 2), (2 1 1), (1 1 2) reflecting planes, indicating the formation of apatite crystalline layer on the surface of the gel glass according to the standard JCPDS file no. (82-1943), [20].

The intensities of these reflection peaks of the HA phase increases with the enhancement of the accumulation of Ca²⁺ and PO₄³⁻ ions on the surface of the gel glass soaked in SBF [21]. There are also some low diffraction maxima at 2θ values 29.3^o, 43.1^o and 48.4^o, that should be assigned to the reflections of (1 0 4), (2 0 2) and (1 1 6) of calcite according to the standard JCPDS card no (81-2027), as shown Fig (4). These results indicate that calcite phase formed during apatite layer growth, that may result from high release of calcium in ions the presence of hydrogen carbonate ions in SBF allowed the precipitation of calcite as described in the following the reaction:-



The calcite formation may be lowered by decreasing CaO concentration in the samples [22].

Evaluation of of apatite crystallinity by XRD (CI_{XRD})

In order to give a semi-quantitative analysis, the changes were observed in the XRD spectra shown in Fig.(4), the measure of crystallinity index (CI_{XRD}) proposed by V. Pearson et al., (1995) [23] was performed.

According to this method, the crystalline index for apatite layer is obtained using the heights of the diffraction peaks $h = (2 1 1)$, $a = (1 1 2)$, $b = (0 0 2)$ and $c = (1 1 1)$, was calculated by the following equation) [23]:-

$$CI_{XRD} = \frac{a + b + c}{h}$$

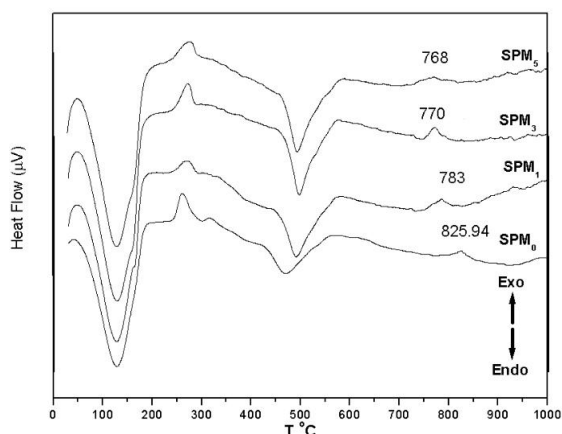


Figure 2. Shows the DTA curves of the gel after drying samples.

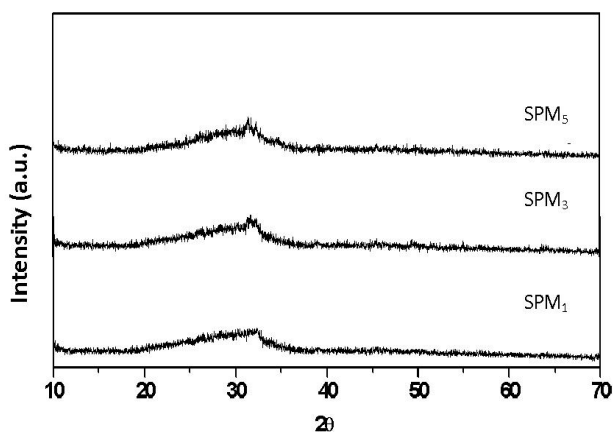


Figure 3. XRD patterns of the gel glass after annealing at 600°C for SPM_1 , SPM_3 , SPM_5 before soaking in SBF.

Fig.(5) shows the dependence of CI_{XRD} of these samples on MgO content. The sample SPM_0 (free MgO) exhibits higher CI_{XRD} than the other samples with different additives of MgO. It is notable that the MgO may be able to enter the forming apatite nuclei and thus inhibits their evolution to tiny apatite crystals. This can be considered for Mg cannot be accommodated in the apatite structure (the apatite lattice) but changes in its physicochemical properties [24].

3.3. FTIR analysis

The FTIR spectra of the prepared samples are shown in Fig. (6). For all glass samples, the band of wavenumber located in the range of 1000–1200 cm^{-1} correspond to the Si–O–Si asymmetric stretching vibration whereas the strong band located at ~ 440–540 cm^{-1} corresponds to the vibrational mode of the bending

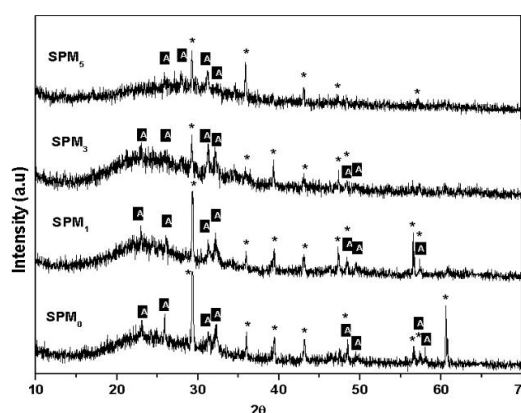


Figure 4. XRD patterns of gel glass after soaking in SBF, The major peaks of calcite (*) ($CaCO_3$) and HA (A) are marked.

of Si–O–Si [25]. The two absorption bands located at ~ 670–740 cm^{-1} corresponds to Si–O symmetric stretch of bridging oxygen (BO) between tetrahedron chains.

Additionally, for silicate glass modified by the incorporation of alkali or/and alkali-earth elements, the shoulder of the spectrum at ~ 870–1040 cm^{-1} is usually related to the stretching modes Si–O with one non-bridging oxygen per SiO_4 tetrahedron (Si–O–NBO) [25]. The band located at 570–600 cm^{-1} is related to asymmetric amorphous PO_3^{-4} bending mode. Moreover, the band in the range ~ 1630–1650 cm^{-1} are commonly due the deformation vibration of the H–O–H group. The broad absorption band corresponding to the carbonate groups CO_3^{2-} was also detected at ~1300–1500 cm^{-1} [26].

Generally, the infrared spectra of poorly crystalline (amorphous) structure differ from those of well crystallized by several features such as broadening. This broadening feature was observed for the main absorption band (Si–O–Si) (s), Fig. (6), indicates the amorphous nature (disorder in the silicate and phosphate network) [27] for all samples before soaking in SBF which was confirmed by XRD. The broadening of the main absorption band in the range 900–1300 cm^{-1} was increased by enhancement of modifier (MgO) content. It is well known, that when a modifier is added to silica, the band at 1100 cm^{-1} will shift to lower wavenumbers (lower frequencies) and covers a broader wavenumbers range by adding greater amount of modifier.

This observed shift can be attributed to the presence of SiO_4 tetrahedron bearing different numbers of non-bridging oxygen, as shown in Fig. (7). These modifications resulting from increasing the MgO content in the system which can be related to the fact that, in silicon network some of the ring structures open

due to break of this silicon network and formation of smaller structures such as short and terminal chains [28].

Fig. (8) Shows FTIR absorption spectra of glass samples after soaking in SBF for 30 days. It can be seen that, there are two new weak bands at 564 cm⁻¹ and 602 cm⁻¹ which are more pronounced in sample (SPM₀) rather than sample (SPM₅). These doublets bands are

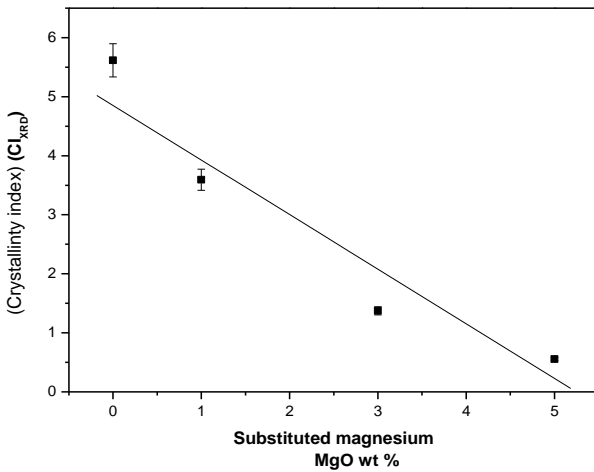


Figure 5. The crystallinity index (CI_{XRD}) of SPM₀, SPM₁, SPM₃ and SPM₅ versus percentage MgO.

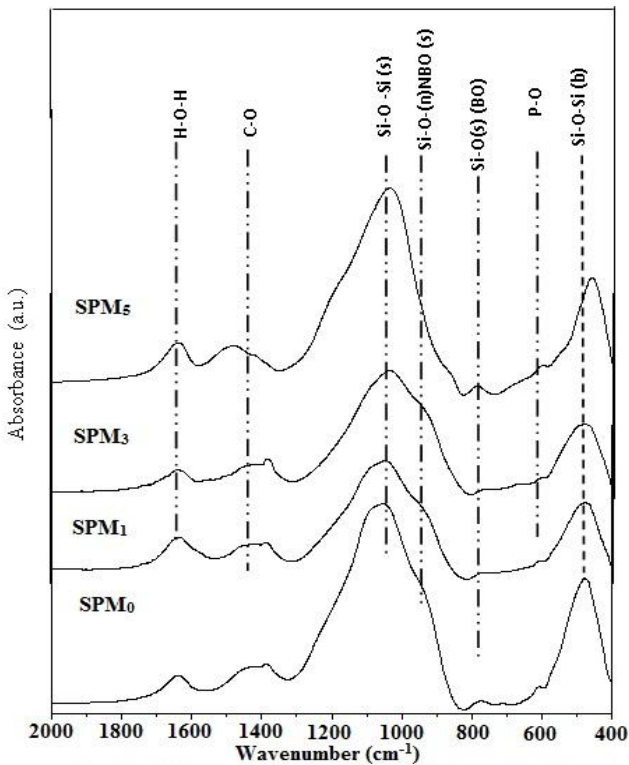


Figure 6. FTIR spectra of synthesized gel glass with different amounts of MgO before soaking in SBF.

usually assigned as crystalline P–O binding vibration mode of PO₄ group tetrahedral. Furthermore, new shoulder at 1150 cm⁻¹ assigned to P–O asymmetric stretching vibration. The three latter bands can be used for monitoring the formation of the HCA layer at the surface of the bioactive glass [29]. Also in addition to that, a band located at 479 cm⁻¹ is assigned to Si–O–Si bending vibration. This band becomes sharper and more intense for all samples after soaking. This indicates that the silicon dissolution reaction was done [30].

Evaluation of apatite crystallinity by FTIR (CI_{FTIR})

Weiner and Bar-Yosef suggested an equation for estimation of the crystallinity index (splitting factor), which is known as concentrations of synthetic amorphous and crystalline apatites. It is indicated that the double peak of phosphate (PO₃⁻⁴) bending frequency at approximately 564 and 602 cm⁻¹ become increasingly separated, or split, as crystallinity increases [31]. The degree of splitting (‘the crystalline index’) is estimated by drawing a baseline from 656 to 512cm⁻¹ and then measuring the heights of the peaks at 602 cm⁻¹ (B), 564 cm⁻¹ (A) and at 595 cm⁻¹ (C) (the lowest point between them). The crystalline index CI_{FTIR} was calculated by the formula [32]:

$$CI_{FTIR} = \frac{A + B}{C}$$

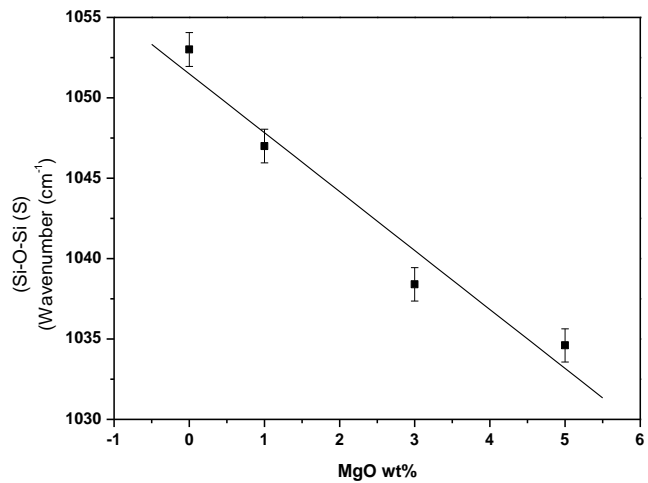


Figure 7. Noticable shift of the main IR band associated with: Si-O-Si(s) as a function of the MgO content.

Figure (9) Shows linear dependence of the crystallinity index (CI_{FTIR}) and MgO additives. This figure reveals that the higher the ratio of magnesium oxide the lower the crystallinity index (CI_{FTIR}). Therefore, the free of MgO sample (SPM₀) exhibits

more order with respect to the sample (SPM_5) with 5wt% MgO. This observation supports the suggestion that, magnesium ions substituted calcium ions at surface of apatite layer formation on gel glass. This substitution may be related to the disorder in the apatite lattice leading to formation of calcium deficient apatite with crystal disarrangement.

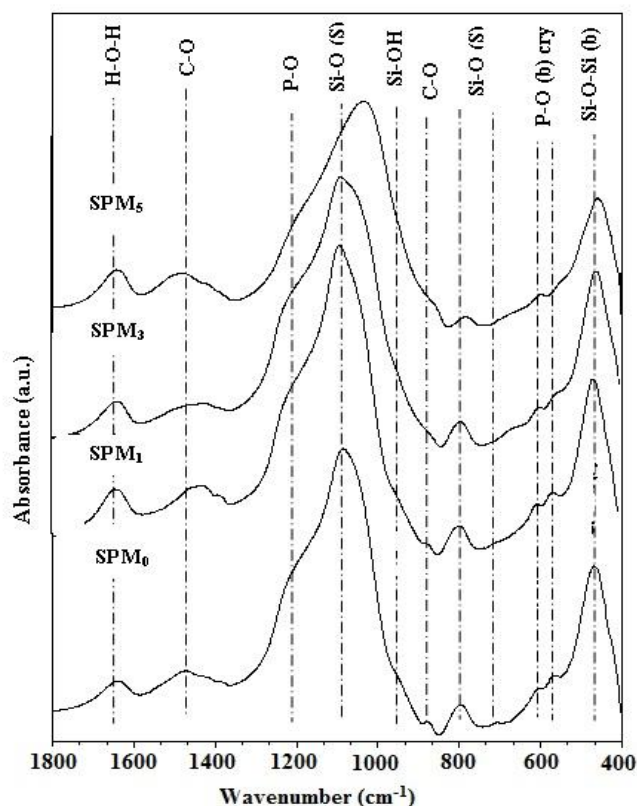


Figure 8. FTIR spectra of synthesized gel glass with different amounts of MgO after soaking in SBF.

Correlation between CI_{XRD} and CI_{FTIR}

Figure (10), reveals the decrement of the crystallinity index of apatite layer formation with increasing the addition of MgO when using two different techniques (X-ray diffractometry CI_{XRD} and FTIR spectroscopy CI_{FTIR}).

It is clear that both CI_{FTIR} and CI_{XRD} follow the same pattern, where the crystallinity decreases by increasing MgO content which reveals a good correlation and sensitivity to the changes in crystallinity^[33], as shown in Fig (11). Finally, the reason for the lack

of crystallization and inhibition of apatite formation is due to the fact that Mg^{2+} ions prefer to interact with PO_4^{3-} ions rather than Ca^{2+} ions in aqueous solution. It follows that Mg^{2+} ions in the SBF form an Mg–Ca-rich layer on the surface of glass samples after soaking for 30 days^[34]. This was incorporated which lowered PO_4^{3-} ion concentration in the SBF, and then decreased the combination rate of PO_4^{3-} with Ca^{2+} . This behavior would reduce the overall rate of seeded calcium phosphate crystallization and markedly delay the transformation of amorphous calcium phosphates to more stable apatite crystal phases^[35].

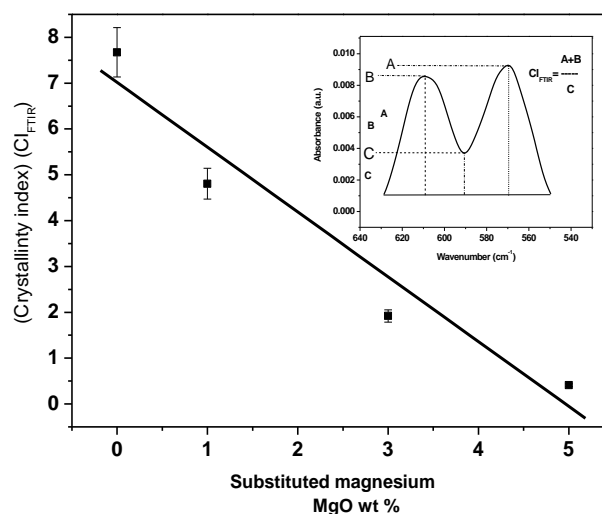


Figure 9. The crystallinity index (CI_{FTIR}) of SPM_0 , SPM_1 , SPM_3 and SPM_5 after soaking in SBF for 30 days versus percentage MgO.

4. Conclusion

Mg-containing bioactive glass is being developed to achieve favorable physicochemical and biological properties for a series of biomedical applications. Mg as an important element of this family of glasses can have different effects on the glass properties. Present results indicate that, with the partial substitution of MgO for SiO_2 in glass composition, the crystallinity of the grown layer was decreased and the formation of apatite-like layer is delayed, confirming that, not all glass surfaces are equally active for nucleation of apatite crystals. Therefore, the results of this study suggest that formation of apatite layer depends on the concentration of MgO which represents decrement in vitro bioactivity.

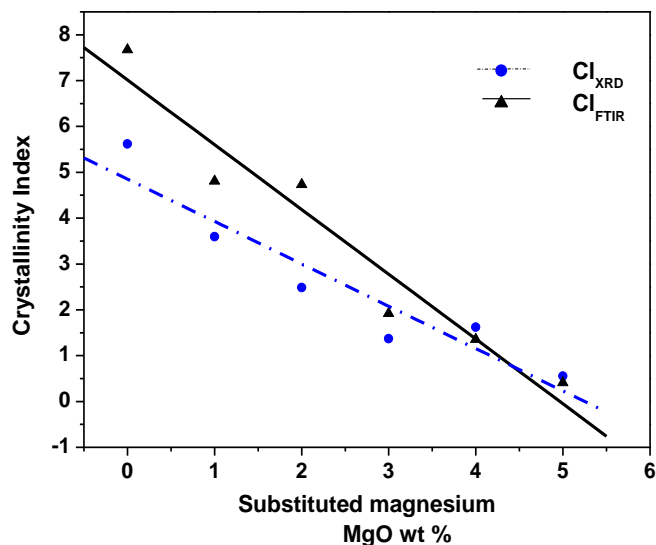


Figure 10. MgO contents and crystallinity index of apatite layer, by two techniques (CI_{XRD} and CI_{FTIR}).

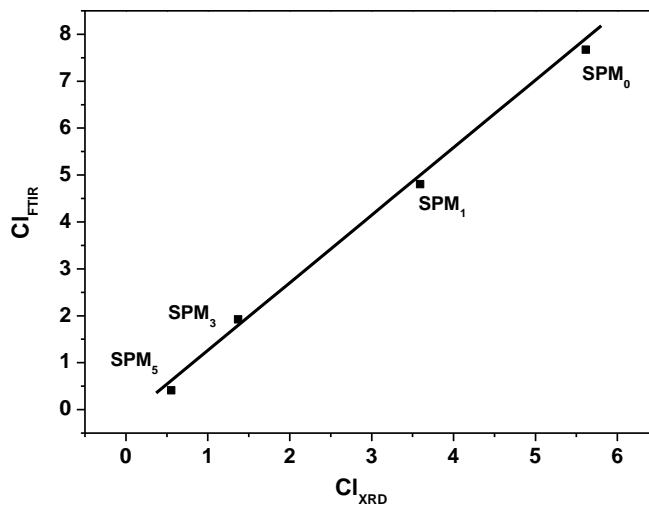


Figure 11. Crystallinity index (CI_{XRD} and CI_{FTIR}) for apatite layer to all samples.

Correspondence to:

Islam E. Soliman

Biophysics branch, Physics Department, Faculty of science, Al-Azhar University, Nasr City, 11884, Cairo, Egypt.

Emails: islamsoloiman@yahoo.com

References

- L.L. Hench, R.J. Splinter, W.C. Allen, T.K. Greenlee, *J. Biomed. Mater. Res.* (1971), Vol. 2, pp. 117-124.
- C. Vitale-Brovarone, E. Verné, M. Bosetti, P. Appendino, M. Cannas, *J. Mater. Sci: Mater. Med.*, (2005), Vol. 16, pp. 909.
- A. Balamurugan, G. Sockalingum, J. Michel, J. Faure, V. Banchet, L. Wortham, S. Bouthors, D. Laurent-Maquin, G. Balossier. *Mater. Lett.*, (2006), Vol. 60, pp. 3752.
- L.L. Hench, I.D. Xynos, J.M. Polak, *J. Biomater. Sci., Polym. Ed.*, (2004), Vol. 15, pp. 543-549.
- M.M. Pereira, A.E. Clark, L.L. Hench, *J. Biomed. Mater. Res.* (1994), Vol. 28, pp. 693-699.
- L.L. Hench, *J. Amer. Ceram. Soc.*, (1991), Vol. 74, pp. 1487-1792.
- L.L. Hench, *J. Amer. Ceram. Soc.*, (1998), Vol. 81, pp. 1705-1728.
- J. Ma, C. Z. Chen, D. G. Wang, X. G. Meng, J. Z. Shi, *J. Sol-Gel Sci. Technol.*, (2010), Vol. 54, pp. 69-76.
- Wei Xia, Jiang Chang, *Mater. Lett.*, (2007), Vol. 61, pp. 3251-325.
- M. Vallet-Regi, C.V. Ragel, A.J. Salinas, *Eur. J. Inorg. Chem.*, (2003), pp. 1029-1035.
- C.T. Wu, J. Chang, J.Y. Wang, S.Y. Ni, W.Y. Zhai, *Biomaterials*, (2005), Vol. 26, pp. 2925-2932.
- A. M. El-Kady, A. F. Ali, R. A. Rizk, M. M. Ahmed, *Ceramics International*, (2012), Vol. 38, pp. 177-188.
- H. Guo, J. Wei, W. Song, S. Zhang, Y. Yan, C. Liu, T. Xiao, *Int. J. Nanomedic.*, (2012), Vol. 73, pp. 613-3624.
- T. Kokubo, H. Takadama, *Biomaterials*, (2006), Vol. 27, pp. 2907-2915.
- A. Oki, B. Parveen, S. Hossain, S. Adeniji, H. Donahue, *J. Biomed. Mater. Res.*, (2004), Vol. 69, pp. 216-21.
- J. R. Jonesa, L. M. Ehrenfried, L. L. Hench, *Biomater.*, (2006), Vol. 27, pp. 964-973.
- Chang-Yeoul Kim, A.R. Jang, B.I. Kim, D.H. Suh, *J. Sol-Gel Sci. Technol.*, (2008), Vol. 48, pp. 336-343.
- K. Balkis, K. Rajasekar, T. Rajasekharan, V. Rajasekharan, *J. Sol-Gel Sci. Technol.*, (2008), Vol. 45, pp. 9-15.
- S. Jalota, S. B. Bhaduri, A. C. Tas, *J. Biomed. Mater. Res. Part B: Appl. Biomater. B*, (2007), Vol. 80, pp. 304-316.
- J.M. Oliveira, R.N. Correia, M.H. Fernandes, J. Rocha, *J. Non-Cryst. Solids*, (2000), Vol. 265, pp. 221-229.
- S.J. Watts, R.G. Hill, M.D. O'Donnell, R.V. Law, *J. Non-Cryst. Solids*, (2010), Vol. 356, pp. 517-524.

22. A. Balamurugan, G. Balossier, S. Kannan, J. Michel, A. H.S. Rebelo, Jose M.F. Ferreira, *Acta Biomaterialia*, (2007), Vol. 3, pp. 255-262.
23. Qi-Zhi Chen, Y. Li, L.Y. Jin, J. M. Quinn, P. A. Komesaroff, *Acta Biomaterialia*, (2010), Vol. 6, pp. 1443-1453.
24. Q. Jie, K. Lin, J. Z. Yifeng, Q. Li, J. Chang, R. Wang, *J. Sol-Gel Sci. Technol.*, (2004), Vol. 30, pp. 49-61.
25. M. Mami, A. Lucas-Girot, H. Oudadesse, R. Dorbez-Sridi, F. Mezahi, E. Dietrich, *Appl. Surf. Science*, (2008), Vol. 254, pp. 7386-7393.
26. V. Pearson, H. Bocherens, J.F. Saliege, F. Paris, V. Zeitoun, M. Gerard, *J. Archaeol. Sci.*, (1995), Vol. 22, pp. 211-21.
27. A. Saboori, M. Sheikhi, F. Moztaarzadeh, M. Rabiee, S. Hesarakhi, M. Tahriiri, N. Nezafati, *Adv. Appl. Ceram.*, (2009), Vol. 108, No. 3, pp. 155-161.
28. H. Aguiar, J. Serra, P. González, B. León, *J. Non-Cryst. Solids*, (2009), Vol. 355, pp. 475-480.
29. Jun Shi, N. M. Alves, J. F. Mano, *Adv. Funct. Mater.*, (2007), Vol. 17, pp. 3312-3318.
30. I. Kansal, D. U. Tulyaganov, A. Goel, M. J. Pascual, J. M. Ferreira, *Acta Biomaterialia*, (2010), Vol. 6, pp. 4380-4388.
31. R. Ciceo Lucacel, A.O. Hulpus, V. Simon, I. Ardelean, *J. Non-Cryst. Solids*, (2009), Vol. 355, pp. 425-429.
32. C. Ohtsuki, H. Kushitani, T. Kokubo, S. Kotani and T. Yamamuro, *J. Biomed. Mater. Res.*, (1991), Vol. 25, (11), pp. 1363-1370.
33. Xia Li, X. Wang, D. He, J. Shi, *J. Mater. Chem.*, (2008), Vol. 18, pp. 4103-4109.
34. G. E. Tiznado-Orozco, R. García-García and J. Reyes-Gasga, *J. Phys. D: Appl. Phys.*, (2009), Vol. 42, pp. 1-13.
35. J. Ma, C.Z. Chen, D.G. Wang, Y. Jiao, J.Z. Shi, *Colloids and Surfaces B: Biointerfaces*, (2010), Vol. 81, pp. 87-95.

12/20/2012